ACS OMEGA

Open Access

http://pubs.acs.org/journal/acsodf

Article

Origin and Formation Mechanism of the Late Permian Black Siliceous Rocks in the Lower Yangtze Region

Xue Gao, Qi Liu, Chaogang Fang,* and Yinghai Guo*

Cite This: *ACS Omega* 2024, 9, 17848−17859

Read Online

ACCESS | Metrics & More | Article Recommendations

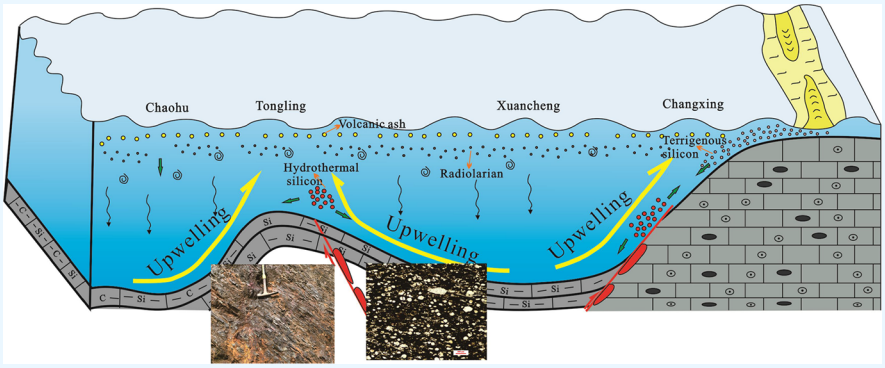

ABSTRACT: The Late Permian witnessed a Permian Chert Event (PCE) and distinctive oceanic geochemical fluctuations, such as an ocean acidification event, large-scale volcanic eruption, and rapid global warming. However, the links between siliceous rock formation mechanism, ocean, and climate changes are rarely discussed. In this article, two well-preserved deeper-water sections of the Dalong Formation from the Lower Yangtze region in southeast China are selected for analysis. To document the coeval oceanic changes, we present thin section authentication, scanning electron microscope (SEM) observation, and multiple geochemical proxies, including total organic carbon contents (TOC), major element contents, trace element contents, and rare earth element contents (REEs). The results show that siliceous rocks are mainly of biological origin in this region. The low content of MgO (0.10−0.94%, mean = 0.36%) in the Fantiansi section of Tongling area indicates that it is affected by regional hydrothermal fluids. The correlation between Al_2O_3/TiO_2, Al_2O_3 versus SiO_2/Al_2O_3, and $TiO_2/\Sigma REEs$ indicates that the Late Permian was greatly influenced by the continuous input of terrigenous materials. The correlations of MnO/TiO_2, La_N/Ce_N, Ce/Ce*, and LREE/HREE imply that the Dalong Formation siliceous rocks were deposited in a continental margin setting. Redox geochemical data (EF_U, EF_{Mo}, and EF_V) imply the water column experienced widespread anoxic/euxinic during the Late Permian, which aided in the preservation of organic matter following biological decay. The accumulation of siliceous rocks is related to South China experiencing a hot tropical climate, coastal upwelling and continental weathering-enriched marine nutrients, fostering high primary productivity, and benefiting abundant siliceous zooplankton. Volcanic and regional hydrothermal activity further enhanced nutrient flux, and the simultaneous ocean acidification event provided favorable chemical conditions for the preservation of silica, leading to the formation of siliceous rocks in the Dalong Formation.

1. INTRODUCTION

Widespread Permian radiolarian and sponge spicule siliceous rocks in the edge of Pangaea, Panthalassa, and Paleo-Tethys Ocean, which are globally correlatable, have been used to define "The Permian Chert Event" (PCE).[1,2] South China is a component of the Tethyan archipelagic ocean system,[3] characterized by the deposition of multilayer siliceous sediments. Several Permian formations in this region include the Gufeng Formation,[4] the Maokou Formation,[5] the Wujiaping Formation,[6] and the Dalong Formation.[7] In particular, the siliceous rocks of the Dalong Formation were deposited during the Permian−Triassic (P−T) transition, a period marked by significant events such as mass extinction, supercontinent amalgamation, oceanic anoxic event, and large-scale volcanic eruption.[8−11] The study on the formation mechanism of the Dalong Formation siliceous rocks may provide valuable insights into understanding these significant events. Additionally, the

Received: October 24, 2023
Revised: March 28, 2024
Accepted: March 29, 2024
Published: April 11, 2024

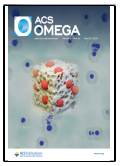

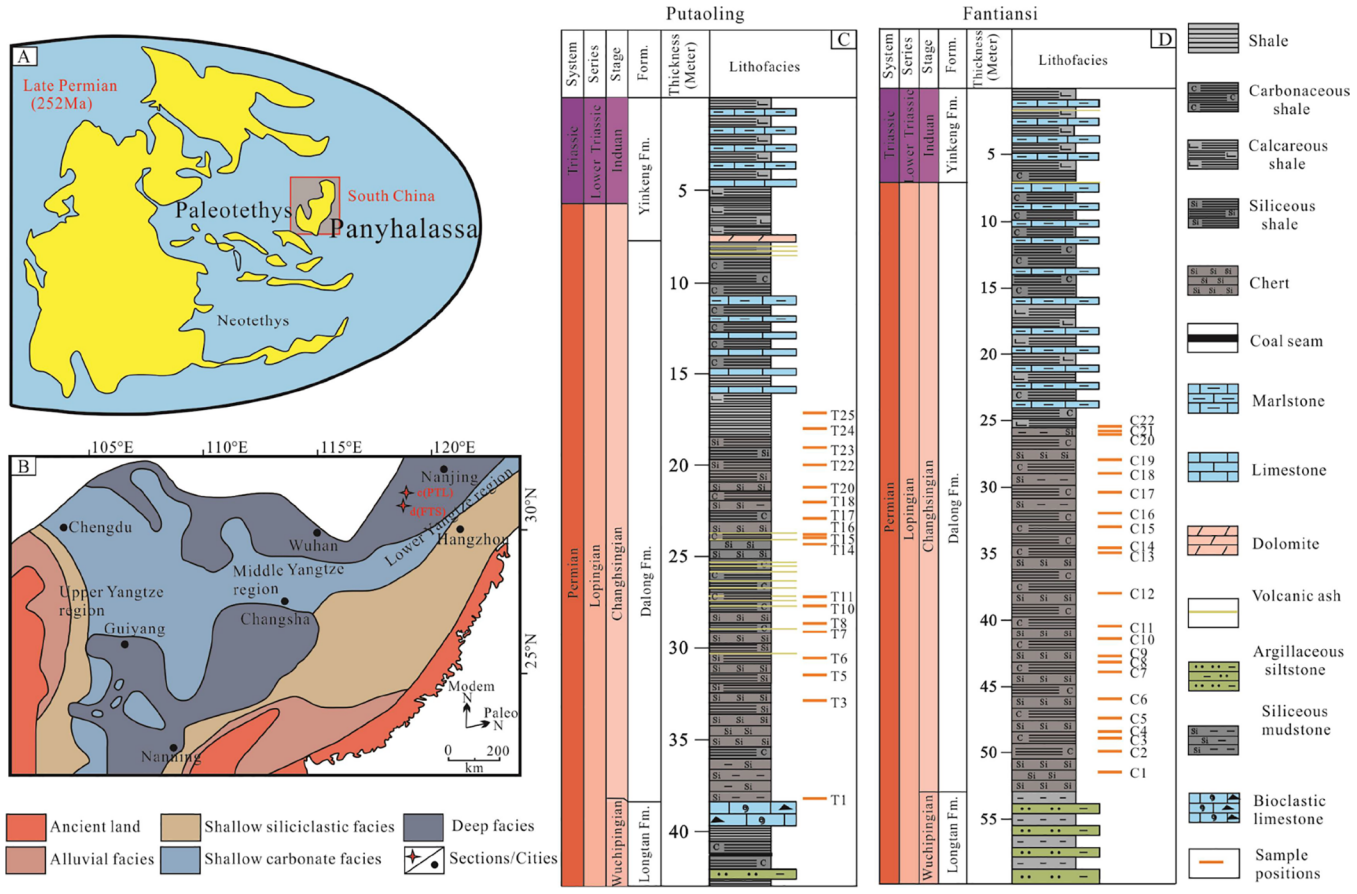

Figure 1. (A) Global paleogeographic map for the Permian−Triassic Boundary interval (ca. 252 Ma). (Base map adapted with permission from ref 28. Copyright 2009 Geological Society of America.) (B) Simplified paleogeography of the South China block during the late Permian and the location of the studied sections. (Base map adapted with permission from ref 29. Copyright 2002 Paleontological Society.) Red stars mark the locations of the Putaoling (PTL) and Fantianshi (FTS) sections. (C) Stratigraphic columns of Putaoling section. (D) Stratigraphic columns of Fantianshi section (short orange lines represent the sample positions for rocks).

siliceous rocks of the Dalong Formation are organic-rich, bearing a strong hydrocarbon significance.[12−15]

The genesis of siliceous rocks in the Dalong Formation has been controversial in South China.[16,17] For example, thin-layer siliceous rocks of the Dalong Formation in the northwestern Sichuan province were considered to be related to hydrothermal sources,[18] whereas the counterparts in southwestern Guizhou were mainly originated from biological silica.[6] Some other cases, which occurred in Guangyuan and Hefeng, were interpreted to have originated from a combination of biological and hydrothermal sources.[19,20] Notably, previous studies, including the above-mentioned, mainly focused on the middle to upper Yangtze region,[6,19,21−24] and the relevant study from the Lower Yangtze region was relatively rare.[13] Moreover, a comparative study between the sections with contrasting interpretations of source and genesis is also lacking, limiting our understanding of the formation environment and processes of the siliceous rocks of the Dalong Formation.

In this contribution, two recently discovered, well-preserved deep-water sections of the Dalong Formation of Chaohu and Tongling in Anhui Province from the Lower Yangtze region are investigated, and the genesis and sedimentary environment of organic-rich siliceous rocks of the Dalong Formation are discussed based on detailed field observation and geochemical analysis of the samples. It holds significance in understanding PCE and the unique paleoceanographic environment at the P-T transition.

2. GEOLOGICAL SETTING

During the P−T transition, South China was situated to the east of the Paleo-Tethys Ocean, in close proximity to the paleoequator. The Lower Yangtze region occupied the northeast edge of South China[25] (Figure 1A), establishing a connection with the Qinling-Dabie Ocean in the northwest and the Cathaysia block in the southeast. Shallow water delta plain environment existed in the Lower Yangtze region during the Wuchiapingian stage, and then the marine transgression began, making a relatively deep-water sedimentary environment during the Changhsingian stage, and a set of rock sequences of black siliceous shale, chert, and carbonaceous shale (Figure 1B). In the early Triassic, slope facies deposition of calcareous shale and limestone interbedding developed due to sea regression.[26,27]

The Putaoling and Fantiansi sections are located in the Lower Yangtze region at Chaohu and Tongling City, in southern Anhui Province. Quarrying operations in these regions have revealed fresh chert, providing an excellent opportunity for examination. Stratigraphically, the geological formations in this vicinity include the Upper Permian Longtan and Dalong Formations alongside the Lower Triassic Yinkeng Formation. There is a notable difference in lithologies between these two sections. The Putaoling section exhibits thin layers of bioclastic limestone at

https://doi.org/10.1021/acsomega.3c08384
ACS Omega 2024, 9, 17848−17859

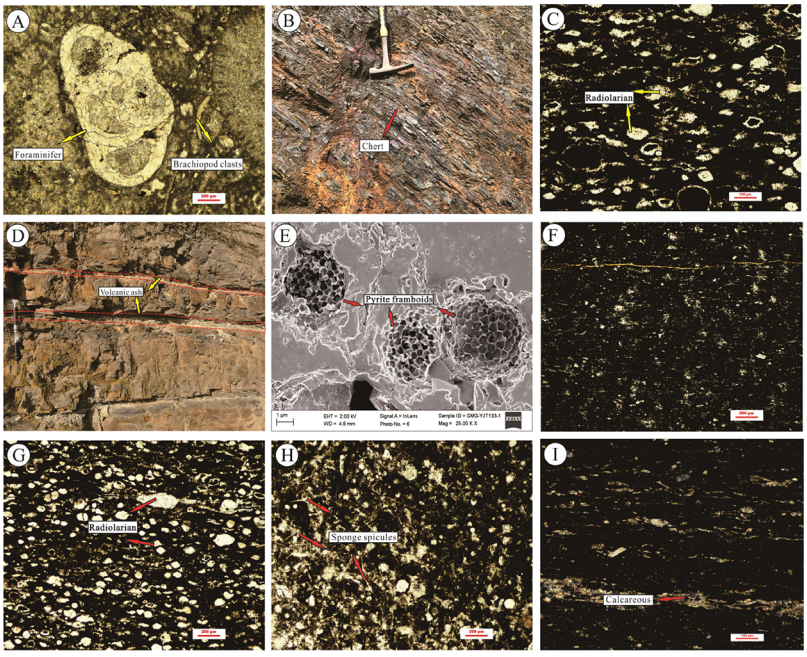

Figure 2. Field and microscopic photographs of typical lithofacies of the Dalong Formation from the Putaoling and Fantiansi sections in the Lower Yangtze region. (A) Bioclastic limestone with foraminifera and brachiopod clasts, Putaoling section. (B) Thin-bedded siliceous rocks, Putaoling section. (C) Thin-bedded chert containing round radiolarian, Putaoling section (plane-polarized light). (D) Volcanic ash layer (arrowed) of the Dalong Formation, Putaoling section. (E) Pyrite framboids under SEM, Putaoling section. (F) Dark carbonaceous shale containing horizontal lamination, Putaoling section (plane-polarized light). (G) Thin-bedded chert containing round radiolarian tests and Fantiansi section (plane-polarized light). (H) Thin-bedded chert containing round sponge spicules, Fantiansi section (plane-polarized light). (I) Calcareous carbonaceous shale, Fantiansi section (plane-polarized light).

the boundary between the Dalong Formation and Longtan Formation (Figure 1C), while the boundary of the lithology transitions from sandy mudstone to siliceous rocks at the Fantiansi section (Figure 1D). In addition, the Fantiansi section was situated at a the edge of the platform during late Permian, and the Putaoling section was located in a relatively stable intraplatform basin, characterized by deeper water.[30]

3. METHODS

A total of 40 fresh siliceous rock samples were selected from the two sections, whose surface layers were removed with the cutter, and the relatively hard parts in the middle without cracks were selected. Subsequently, the samples were cut into pieces using a hammer and further pulverized into 200 or 80 mesh-sized powders using an agate ring mill. The sample with 80 mesh was used for the measurement of total organic carbon (TOC) and was conducted with a CS-230 carbon−sulfur analyzer in East China Oil and Gas Company of SINOPEC. The sample with 200 mesh was mainly used for the testing of main and trace elements, and REEs were performed in the Testing Center of Nanjing Institute of Geology and Mineral Resources, with a wavelength-dispersive X-ray fluorescence spectrometer (WDXRF) and Panalytical Axios for main elements (test progress is 5% better than others) and an ICAPQ inductively coupled plasma source mass spectrometer made by Thermo Fisher Scientific for trace elements and REEs, with analytical error less than 5%.

4. RESULTS

4.1. Lithology. The Longtan Formation of the Putaoling section consists of a series of coal-bearing clastic rocks. The boundary between the Longtan Formation and the Dalong Formation is marked by a bioclastic limestone (Figure 2A). The middle and lower parts of the Dalong Formation primarily comprise black cherts (Figure 2B), carbonaceous siliceous shale, and carbonaceous shale. The cherts are abundant in radiolarian and sponge spicule fossils (Figure 2C) and are partially interbedded with gray yellow and yellowish volcanic ash (Figure 2D). Pyrite framboids (Figure 2E) are commonly observed by SEM. The upper part of the Dalong Formation consists of dark gray medium-thin layer of micrite limestone and muddy limestone, as well as carbonaceous shale (Figure 2F). The lithology at the Fantiansi section changes from a combination of silty sandstone and mudstone at the top of the Longtan Formation to cherts of the Dalong Formation. The Dalong Formation can be further divided into two parts based on lithology. The lower part consists mainly of black thin-layer cherts, siliceous shales, and carbonaceous shales. The lower part also contains a significant amount of radiolarian (Figure 2G) and sponge spicule (Figure 2H). The upper part of the Dalong Formation consists of a combination of muddy limestone, limestone, and calcareous carbonaceous shale (Figure 2I). The difference in lithology between the two sections shows that the cherts in the Fantiansi section are more developed than in the Puguling section.

4.2. Major Element Characteristics. Major element contents are shown in Table 1. SiO_2 content of the Putaoling section is 51.68−79.50% with a mean of 62.73%. The average contents of Al_2O_3, CaO, K_2O, Fe_2O_3, and MgO are 12.18, 4.17, 2.55, 3.61, and 1.43%, respectively; Other oxide contents do not reach 1%. The Fantiansi section has a higher SiO_2 content than the Putaoling section, with the mean of 82.32%, while the contents of Al_2O_3, CaO, K_2O, Fe_2O_3, and MgO are relatively low, with average contents of 4.99, 0.29, 0.81, 1.85, and 0.36%.

https://doi.org/10.1021/acsomega.3c08384
ACS Omega 2024, 9, 17848−17859

Table 1. Total Organic Carbon (%), Major Element (%), and Relevant Parameters of the Dalong Formation in the Putaoling and Fantiansi Sections of the Lower Yangtze Region

sample	TOC	Al_2O_3	CaO	Fe_2O_3	K_2O	MgO	MnO	Na_2O	P_2O_5	SiO_2	TiO_2	Si_{XS}	Al/(Al + Fe + Mn)
T25	0.85	15.14	0.18	1.54	2.81	1.15	0.00	1.10	0.05	68.18	0.50	6.95	0.88
T24	1.76	15.89	0.17	3.88	3.11	1.23	0.00	0.76	0.11	64.02	0.55	3.78	0.76
T23	5.00	8.55	0.36	2.74	1.54	0.58	0.00	0.55	0.07	79.50	0.34	23.08	0.70
T22	5.42	14.78	4.22	4.25	2.73	1.59	0.07	0.92	0.10	59.71	0.50	3.58	0.72
T20	2.70	16.31	2.09	3.78	3.21	1.76	0.05	0.60	0.13	63.26	0.57	2.72	0.76
T18	5.96	11.24	6.60	3.31	2.14	1.36	0.02	0.74	0.12	61.19	0.39	10.11	0.72
T17	4.03	10.16	8.42	3.75	1.98	1.13	0.02	0.62	0.17	57.73	0.36	10.27	0.67
T16	8.20	10.75	7.24	5.45	2.08	1.04	0.02	0.91	0.16	52.01	0.40	6.61	0.60
T15	1.84	10.36	4.70	3.53	2.02	0.85	0.01	0.80	0.12	60.83	0.40	11.38	0.69
T14	5.16	8.59	4.15	4.34	1.72	0.75	0.01	0.56	0.15	62.01	0.32	14.85	0.60
T11	10.83	10.68	9.14	5.38	2.45	1.03	0.03	0.47	0.14	51.68	0.40	6.57	0.60
T10	6.59	15.30	3.35	2.86	3.49	1.76	0.04	0.61	0.17	62.09	0.51	3.84	0.80
T8	6.03	13.04	4.31	3.60	2.83	2.34	0.05	0.67	0.10	62.41	0.47	7.72	0.73
T7	5.82	15.76	4.10	3.26	3.49	1.73	0.03	0.71	0.33	60.07	0.48	2.13	0.78
T6	5.67	12.22	5.69	3.26	2.67	1.70	0.05	0.51	0.13	63.76	0.39	9.69	0.74
T5	6.24	8.33	2.68	2.61	1.72	1.16	0.03	0.51	0.06	76.35	0.31	21.98	0.71
T3	13.20	13.82	3.92	3.82	2.98	2.43	0.06	0.68	0.10	61.28	0.53	5.90	0.73
T1	4.58	13.66	3.67	3.61	2.89	2.18	0.05	0.79	0.09	63.01	0.43	6.96	0.74
C22	6.77	4.24	0.48	0.95	0.55	0.45	0.01	0.68	0.03	84.89	0.17	32.71	0.77
C21	11.42	3.55	1.33	1.03	0.42	0.94	0.01	0.65	0.02	83.71	0.15	33.28	0.72
C20	9.35	4.59	0.21	0.99	0.68	0.31	0.01	0.69	0.03	84.89	0.18	32.13	0.78
C19	4.13	4.65	0.69	0.98	0.66	0.59	0.01	0.72	0.05	85.92	0.17	32.51	0.78
C18	2.29	5.90	0.29	1.35	0.96	0.34	0.00	0.54	0.20	78.94	0.25	27.18	0.77
C17	4.20	8.89	0.18	11.96	1.28	0.39	0.00	<0.1	0.06	70.81	0.67	18.47	0.36
C16	4.01	8.49	0.12	1.58	1.20	0.43	0.00	1.18	0.16	72.41	0.30	19.87	0.80
C15	13.58	10.32	0.53	1.86	1.66	0.56	0.00	1.30	0.55	62.61	0.39	12.28	0.81
C14	6.09	7.99	0.06	1.82	1.49	0.52	0.00	0.66	0.03	72.93	0.33	20.94	0.77
C13	6.64	8.80	0.11	2.46	1.81	0.53	0.00	0.32	0.26	72.18	0.33	19.25	0.73
C12	7.95	9.13	0.25	3.85	1.94	0.49	0.00	0.37	0.36	68.72	0.36	17.09	0.64
C11	4.95	5.06	0.07	2.91	0.84	0.32	0.01	0.18	0.23	79.83	0.20	28.98	0.57
C10	13.12	8.84	0.23	1.18	1.67	0.60	0.00	0.29	0.39	71.57	0.35	18.91	0.85
C9	2.71	2.56	0.13	0.69	0.39	0.18	0.02	<0.1	0.16	91.21	0.09	38.43	0.73
C8	2.05	1.47	0.12	1.06	0.21	0.12	0.02	<0.1	0.06	92.91	0.09	41.01	0.51
C7	1.69	1.64	0.12	1.16	0.24	0.14	0.03	<0.1	0.07	93.08	0.08	40.81	0.51
C6	7.04	2.77	0.72	0.21	0.57	0.23	0.01	<0.1	0.02	80.18	0.29	32.92	0.91
C5	2.25	2.12	0.08	0.50	0.34	0.17	0.01	<0.1	0.05	92.95	0.10	39.97	0.76
C4	0.99	2.73	0.17	1.32	0.26	0.13	0.03	<0.1	0.05	92.80	0.12	38.88	0.61
C3	2.07	1.56	0.09	0.64	0.18	0.10	0.02	<0.1	0.06	94.07	0.08	41.41	0.64
C2	1.59	1.43	0.17	0.84	0.18	0.11	0.01	<0.1	0.06	94.16	0.05	41.66	0.56
C1	0.58	2.96	0.26	1.43	0.37	0.19	0.01	<0.1	0.16	90.22	0.14	37.30	0.61

4.3. Trace Element Characteristics. The trace element contents of the Putaoling section and the Fantiansi section of Dalong Formation are shown in Table 2, with a mean content value of the trace elements in Post Archaean Australian Shale (PAAS)[31] and to ensure comparability of the normalization results, enrichment factors (EFs) are commonly employed. The formula used is EF element $_X = X/Al_{sample}/X/Al_{standard.}$[32,33] If EF_X is greater than 1, it indicates an enrichment of element X relative to the standard shale. If EF_X is less than 1, it indicates depletion.[34]

Enrichment factors of V (EF_V) are slightly high, ranging between 0.8 and 26.1 (average 8.1). In contrast, U and Mo (EF_V and EF_{Mo}) are the most enriched (EF_U average to 37.5, and EF_{Mo} average to 299.6). Micronutrients such as Ni, Cu, Zn, and P show enrichment factors (EF_{Ni}, EF_{Cu}, EF_{Zn}, and EF_P) ranging from 0.2 to 11.8 (average 3.8), 0.2−7.2 (average 2.4), 0.3−9.8 (average 1.9), and 0.4−7.5(average 2.5), respectively (Figure 3).

4.4. Rare Earth Element (ΣREE) Characteristics. The ΣREE in the black siliceous rocks of Dalong Formation at the Putaoling section ranges from 110.7 to 210.0 ppm, with a mean content of 149.0 ppm (Table 2). In contrast, the ΣREE content at the Fantiansi section is significantly lower, ranging from 17.4 to 147.2 ppm, with an average content of 64.4 ppm. The content of ΣLREE/ΣHREE (L/H) in the Putaoling section is 7.1−12.2, with the average content of 8.8, and the content of L/H in the Fantiansi section is 2.9−17.1, with the average content of 6.8.

The Ce/Ce* values for siliceous rocks within the Dalong Formation at the Putaoling section exhibit a range from 0.87 to 0.96, averaging at 0.92. Similarly, in the Fantiansi section, the Ce/Ce* values vary between 0.79 and 0.94, with a mean value of 0.88. Within the Putaoling section, the Eu/Eu* ratios range from 0.71 to 0.93, with an average of 0.80, while in the Fantiansi section, these ratios range from 0.67 to 1.11, with an average of 0.83. Both the Dalong Formation siliceous rocks in the Putaoling

https://doi.org/10.1021/acsomega.3c08384
ACS Omega 2024, 9, 17848−17859

Table 2. Trace Element Content (ppm), REE Content (ppm), and Relevant Parameters of the Dalong Formation in the Putaoling and Fantiansi Sections of the Lower Yangtze Region

sample	EF_{Cu}	EF_{Ni}	EF_{Zn}	EF_{P}	EF_{Mo}	EF_{V}	EF_{U}	ΣREE	LREE/HREE	Ce/Ce*	Eu/Eu*	La_N/Ce_N
T25	0.2	0.8	0.3	0.38	211.0	4.9	23.6	169.7	12.2	0.9	0.7	1.1
T24	0.8	1.2	1.0	0.81	163.0	5.1	18.6	162.0	11.3	0.9	0.8	1.1
T23	1.3	2.3	1.2	1.01	532.8	14.1	42.0	111.9	7.3	0.9	0.9	1.2
T22	1.7	1.9	1.6	0.81	35.4	1.3	11.8	166.3	8.3	0.9	0.9	1.1
T20	1.9	1.6	1.3	0.93	28.5	1.1	7.3	182.2	7.8	0.9	0.7	1.1
T18	2.8	2.1	1.3	1.28	180.0	3.7	19.0	124.2	8.9	0.9	0.8	1.1
T17	3.9	4.1	1.8	1.95	253.2	7.2	33.1	130.5	7.8	0.9	0.9	1.1
T16	4.0	5.7	2.0	1.72	833.5	14.5	48.5	121.0	8.0	0.9	0.9	1.1
T15	2.9	4.6	1.1	1.42	1310.3	11.9	58.6	120.6	8.4	0.9	0.8	1.0
T14	4.8	8.0	2.0	2.03	1248.0	26.1	60.2	110.7	7.6	0.9	0.7	1.1
T11	2.8	3.2	1.1	1.53	633.6	10.4	48.6	133.7	7.1	0.9	0.9	1.1
T10	1.7	1.3	1.2	1.32	47.3	1.3	18.7	182.0	9.4	1.0	0.8	1.1
T8	1.7	1.8	1.6	0.95	17.1	1.0	10.4	135.8	9.6	0.9	0.7	1.1
T7	2.6	1.9	1.7	2.51	33.0	1.3	29.3	210.0	8.0	0.9	0.7	1.1
T6	1.8	1.5	1.3	1.31	14.1	0.8	11.7	144.7	9.3	0.9	0.9	1.1
T5	1.8	2.2	2.0	0.85	19.5	0.9	18.5	126.6	7.6	0.9	0.7	1.1
T3	1.7	1.8	1.5	0.85	10.1	1.1	23.8	160.7	9.7	0.9	0.7	1.1
T1	1.4	1.2	1.5	0.75	11.8	0.8	9.3	152.7	10.2	0.9	0.8	1.1
C22	1.5	4.4	1.2	0.90	190.6	8.0	17.2	30.1	6.7	0.9	0.8	1.1
C21	3.0	6.8	2.0	0.64	102.3	7.7	22.8	35.6	6.4	0.9	0.7	1.1
C20	2.0	4.6	1.9	0.89	46.2	4.6	25.4	60.7	6.5	0.9	0.7	1.1
C19	2.3	3.6	1.7	1.31	27.6	1.3	17.4	68.7	7.5	0.9	0.8	1.1
C18	1.9	5.1	2.0	4.01	76.5	8.3	31.7	55.4	5.4	0.9	0.9	1.1
C17	0.5	0.2	0.4	0.83	51.5	2.9	9.6	130.7	17.1	0.9	0.8	1.1
C16	0.9	3.3	1.5	2.21	110.9	12.8	27.9	97.2	6.5	0.8	0.8	1.3
C15	0.8	3.0	1.4	6.42	157.0	17.3	44.9	139.2	6.6	0.9	0.8	1.1
C14	0.7	2.5	0.7	0.43	216.7	18.6	17.4	83.4	9.2	0.9	0.8	1.1
C13	1.8	3.2	0.8	3.50	70.4	6.9	17.7	70.3	7.5	0.9	0.9	1.2
C12	1.6	2.4	0.9	4.67	256.7	10.2	31.8	96.2	6.9	0.9	1.0	1.1
C11	3.5	3.5	0.9	5.53	392.0	9.9	45.1	66.3	5.9	0.9	0.9	1.1
C10	1.2	1.4	0.7	5.32	179.1	12.0	47.3	147.2	7.6	0.9	0.8	1.1
C9	2.1	2.1	1.6	7.53	392.0	11.2	39.0	33.3	5.5	0.9	1.0	1.1
C8	7.2	7.6	4.7	5.04	1425.6	20.0	50.8	17.4	5.7	0.9	1.1	1.0
C7	2.6	4.2	2.9	5.40	408.3	10.6	158.4	29.3	4.9	0.9	0.7	1.0
C6	1.0	9.7	0.9	0.99	284.1	14.4	89.3	71.1	8.5	0.9	0.8	1.2
C5	1.4	2.1	0.9	2.54	253.9	11.2	64.8	29.4	5.6	0.9	0.9	1.1
C4	7.1	11.8	9.8	1.97	323.2	8.3	57.0	40.6	2.9	0.8	0.9	1.3
C3	4.4	6.4	3.0	4.37	490.2	7.0	49.3	22.7	5.9	0.8	1.0	1.3
C2	4.5	9.5	3.8	4.86	751.2	10.6	58.2	29.4	3.8	0.8	0.7	1.1
C1	3.4	8.1	5.9	6.26	194.2	4.9	83.5	63.4	5.9	0.8	0.9	1.2

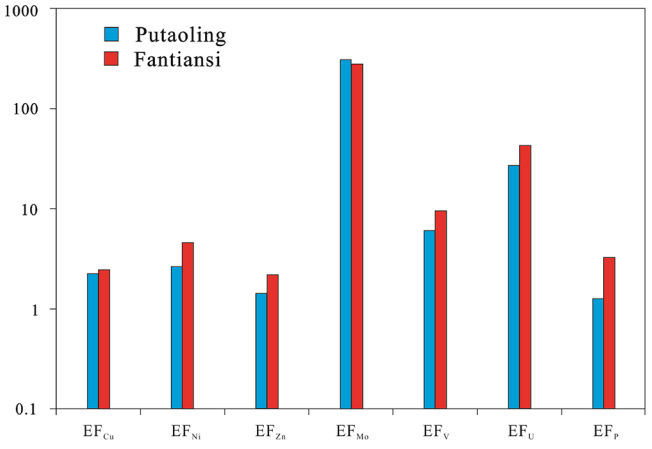

Figure 3. Trace element enrichment factors (EFs) of siliceous rocks from the Putaoling and Fantiansi sections relative to PAAS.

section and the Fantiansi section display weak negative anomalies in both Ce and Eu.

5. DISCUSSION

5.1. Sources of Silica. The origin of silica, the depositional environment, and formation mechanisms are three fundamental areas of interest in research on siliceous rocks.[1,4,35] The silicon sources in siliceous rocks are mainly divided into the following three forms. (1) Terrigenous debris, which refers to the chemical breakdown products of silicate or aluminosilicate minerals resulting from continental weathering.[36−38] (2) Siliceous organisms, such as radiolarians and sponge spicules.[2,4,39] (3) Deep-sourced materials, including those resulting from marine hot water vent activity, and marine hydrolysis of volcanic materials.[5,17,38,40]

The Al_2O_3 content of the black siliceous rocks of the Putaoling section is 8.33−16.31%, with TiO_2 content (0.31−0.57%) and SiO_2/Al_2O_3 content (3.81−9.30). The Al_2O_3

https://doi.org/10.1021/acsomega.3c08384
ACS Omega 2024, 9, 17848−17859

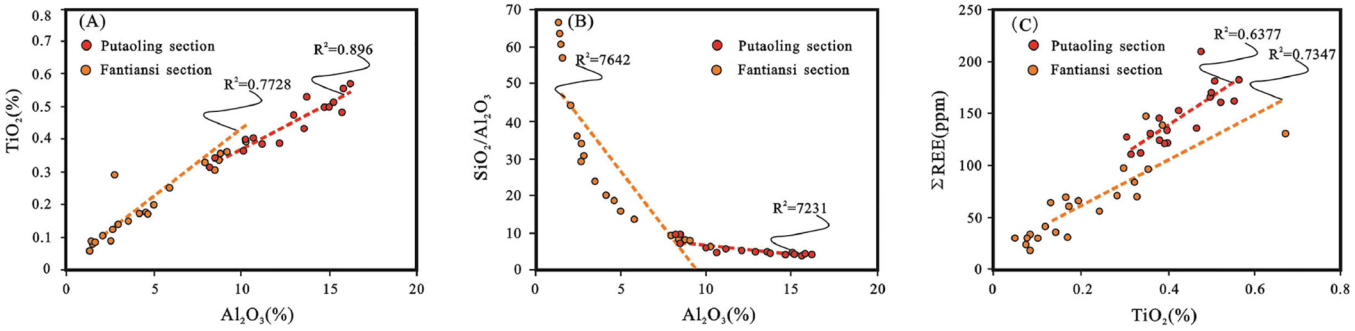

Figure 4. Cross-plots of the Al_2O_3 versus TiO_2 (A), Al_2O_3 versus SiO_2/Al_2O_3 (B), and TiO_2 versus ΣREEs (C) from the Putaoling and Fantiansi sections.

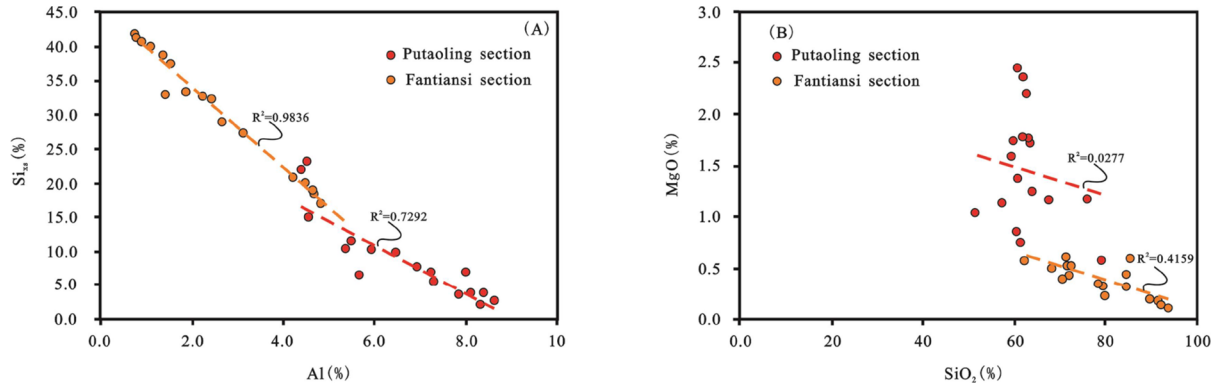

Figure 5. Cross−plots of the Al versus Si_{xs} (A) and SiO_2 versus MgO (B) for the Putaoling and Fantiansi sections from the Lower Yangtze region.

content of the black siliceous rocks of the Fantiansi section is 1.43−10.32%, with the TiO_2 content (0.05−0.67%) and SiO_2/Al_2O_3(6.07−65.98), which is lower than pure siliceous rocks (SiO_2/Al_2O_3 is 80−1400). Al_2O_3 and TiO_2 exhibit a strong positive correlation, while SiO_2/Al_2O_3 and Al_2O_3 demonstrate a notable negative correlation (Figure 4A,B). These findings are commonly interpreted as indicating a higher presence of clay-rich sediments from Terrigenous input.[41] Total content of ΣREEs is also considered to originate mainly from clay mineral in terrestrial material.[42,43] And the strong correlation between TiO_2 and ΣREEs further indicates the higher contribution of terrigenous clastic sediments in the source region (Figure 4C).

Excessive silicon content (Si_{XS}) refers to the SiO_2 content that is higher than that found in a normal clastic sedimentary environment.[44] It can be calculated using the formula $Si_{XS} = Si_{sample} - [(Si/Al)_{background} \times Al_{sample}]$, where $(Si/Al)_{background}$ represents the average shale ratio of 3.11.[45] This ratio is commonly used to study the origin of silicon in organic-rich mudstone.[20,44,46] Microscopic observation reveals that the Putaoling section and the Fantiansi section are mainly biologically sedimentary siliceous rocks. Silica content is generally above 60%, mainly composed of micrograined quartz. Microfossils are mainly radiolarian and sponge spicule (accounting for about 5∼35% of the total area). Radiolarian is round shaped and starlike scattered (Figure 2C,G) with wide distribution, while sponge spicule is needle-shaped with limited distribution (Figure 2H), and whose interior is filled with silica and quartz, with particle size generally less than 0.20 mm. Meanwhile, The Si_{XS} content in the Putaoling section ranges from 2.72 to 21.98%, with an average content of 8.78%. In the Fantiansi section, the Si_{XS} content ranges from 12.28 to 41.66%, with an average content of 30.27%. The obvious negative correlation between the excessive silicon and Al content in this research (Figure 5A) can indicate that Si_{XS} is not caused by clay mineral transformation.

The MgO content is very low in the modern midocean ridge hydrothermal system, which tends to be zero the 350 °C in the East Pacific midocean-ridge hydrothermal system (350 °C), and the increase of which is the result of hot water and seawater mixing.[47] Therefore, the MgO content is relatively low in hot water sedimentary siliceous rocks, which are negatively associated with the SiO_2 content.[48] The MgO content in siliceous rocks of the Putaoling section is 0.58−2.43%, with an average content of 1.43%, which is relatively high, with no significant correlation with the SiO_2 content. The MgO content in siliceous rocks of the Fantiansi section is 0.10−0.94%, with an average content of 0.36%, showing very low MgO content, with a moderate negative correlation with the SiO_2 content (Figure 5B), implying that part of the silicon in the Fantiansi section is derived from hydrothermal fluids.

Major element analysis is a valuable tool for distinguishing the origin of cherts influenced by the hydrothermal activity. Cherts that have been affected by hydrothermal processes generally exhibit higher concentrations of Fe and Mn.[49] The Al content in cherts is considered to vary based on siliciclastic input.[50] A value of Al/(Al + Fe + Mn) greater than 0.6 indicates a biogenic origin, while a value lower than 0.01 suggests a hydrothermal origin.[49]

The Al/(Al + Fe + Mn) values of black siliceous rocks in the Putaoling section range from 0.60 to 0.88, with an average value of 0.72. In the Fantiansi section, the Al/(Al + Fe + Mn) values range from 0.36 to 0.91, with an average value of 0.69. These results show that the Dalong Formation in the Putaoling section is primarily formed through biological sedimentation, while the Fantiansi section shows evidence of being influenced by the

https://doi.org/10.1021/acsomega.3c08384
ACS Omega 2024, 9, 17848−17859

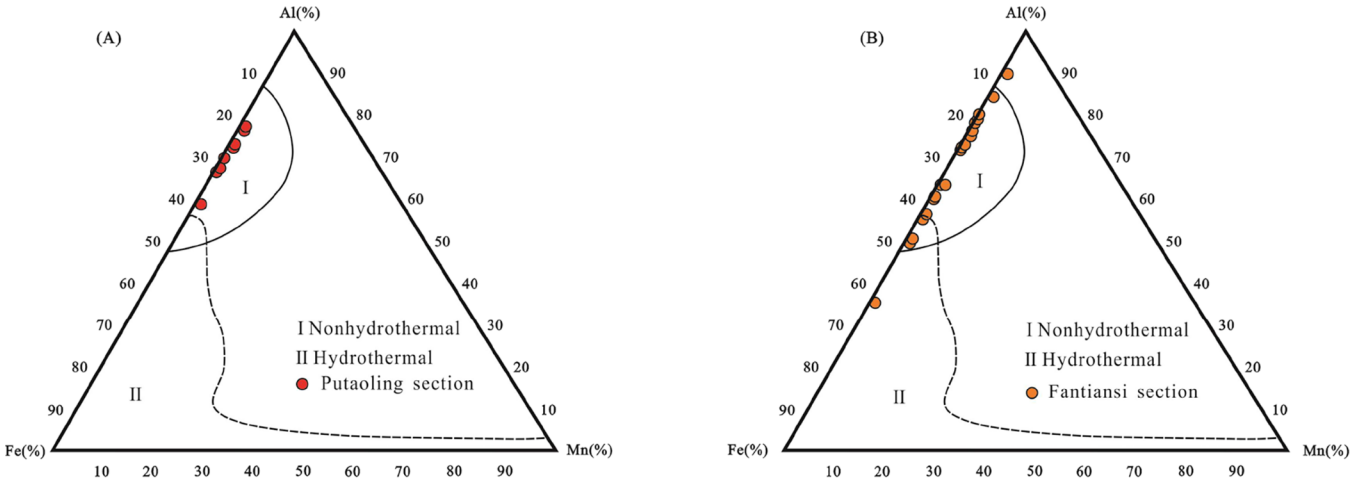

Figure 6. Al−Fe−Mn diagram of Dalong Formation in Putaoling section (A) and Al−Fe−Mn diagram of Dalong Formation in Fantiansi section (B) for the thin-bedded siliceous rocks of the Dalong Formation. (Base map adapted with permission from ref 55. Copyright 1986 Elsevier.)

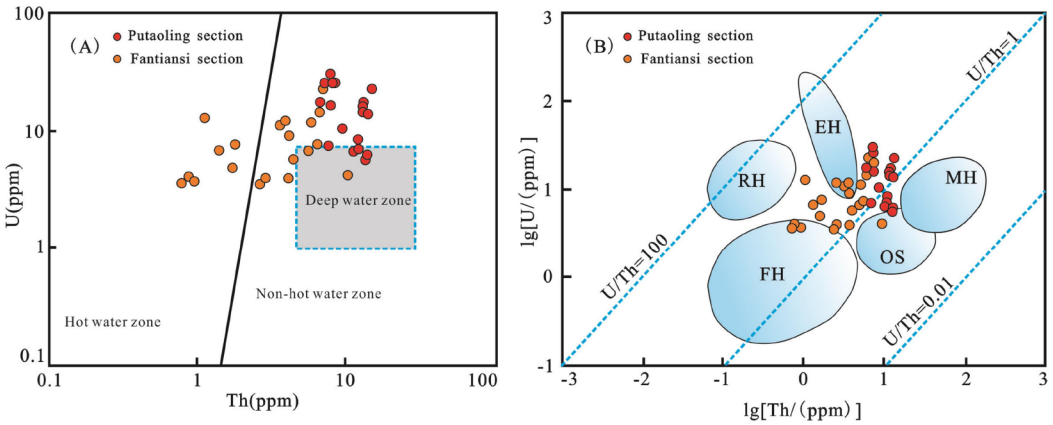

Figure 7. Cross-plots of the U versus Th (A) and LgU versus LgTh (B) of Dalong Formation in Putaoling and Fantiansi sections. [(A) Base map adapted with permission from ref 54. Copyright 2012 Elsevier. (B) Base map adapted with permission from ref 53. Copyright 2018 Elsevier.] RH—red sea hydrothermal sediment; EH—hydrothermal sediment of Pacific Eastern ridge; FH—precontemporary hydrothermal sediment; OS—common deep-sea sediment; AH—bauxite sediment; and MH—deep-sea ferromanganese nodules.

hydrothermal fluid origin. When analyzing the Al−Fe−Mn discrimination diagrams,[49−51] the sample points of the Putaoling section are categorized under the biological-sedimentary area (Figure 6A). A few sample points of the Fantiansi section are classified under the hot water sedimentary area or the biological and hot water mixing area (Figure 6B). Meanwhile, the correlation between trace elements Th and U can also be used to distinguish the effect of hot water on sediments.[52−54] In nonhydrothermal sediments (such as normal water bodies and deep-sea sediments), a significant amount of Th is drawn from seawater due to the sediment accumulation rate. However, in hot water sedimentation, deposits accumulate quickly and cannot extract Th from the seawater, resulting in a relatively higher concentration of U. The distribution pattern of the Dalong Formation black siliceous rocks in the Putaoling section, as depicted in Figure 7A, indicates that the majority of points are found in the normal water area, with only small points in the deep-water deposition area. Similarly, in the Fantiansi section, most of the points are located in the normal water area, with a few points in the hot water sedimentation area and the deep-water deposition area. This suggests that the Dalong Formation black siliceous rocks in the Fantiansi section have been somewhat influenced by hot water. Additionally, as depicted in Figure 7B, the projection point of the Putaoling section mainly falls within the normal marine environment, while a few points in the Fantiansi section are located in the Iron−Manganese hydrothermal sedimentary area and the East Pacific hot water sedimentation area of the East Pacific Ocean. This further supports the notion that the Dalong Formation siliceous rocks in the Fantiansi section have been affected by hot water sedimentation. The Permian cherts in South China display pronounced spatial heterogeneity, primarily attributed to their diverse proximity to the hydrothermal activity of the E'meishan Large Igneous Province (ELIP) and deep faults. During the late Permian,[56,57] the ELIP triggered more volcanic and hydrothermal activity within the middle-upper Yangtze region.[5,16,57]

5.2. Sedimentary Environment. The separation and enrichment of the chemical composition of rocks are influenced by the sedimentary environment. By analyzing the element geochemical characteristics in rocks, the sedimentary environment can be identified.[52] Parameters such as the MnO/TiO_2 and Ce anomalies (Ce/Ce*) can serve as significant indicators to determine the paleogeographic location of the sedimentary basin. Generally, $MnO/TiO_2 < 0.5$ indicates continental slope or marginal sea deposition on the continental margin, and MnO/TiO_2 between 0.5 and 3.5 shows oceanic bottom sedimenta-

https://doi.org/10.1021/acsomega.3c08384
ACS Omega 2024, 9, 17848−17859

tion.[51] In the Putaoling Section, the MnO/TiO_2 value of the black siliceous rocks in the Dalong Formation ranges from 0.0036 to 0.1323%, with an average value of 0.0657%. In the Fantiansi section, the MnO/TiO_2 value ranges from 0.0026 to 0.3210%, with an average value of 0.0942%. These values suggest that the cherts of the Dalong Formation likely formed in a continental slope or marginal sea deposition rather than in open water.

The composition of REEs in chert and shale can provide valuable insights into the depositional environment.[58] For instance, the Ce anomaly is utilized to ascertain the relative distance from the terrestrial sediment input. Murray et al.[59,60] focused on the Ce anomaly in cherts from the Franciscan Complex in California. The mean values ranged from 0.9 to 1.30 at a continental margin, 0.6 in an ocean-basin setting, and 0.29 were identified at a spreading ridge. The Ce/Ce* value of Dalong Formation siliceous rocks in the Putaoling section ranges from 0.87 to 0.96 (average 0.92). In the Fantiansi section, the Ce/Ce* value is 0.79−0.94 (average 0.88), showing that the siliceous rocks were deposited near the continental margin. The La_N/Ce_N ratio is a valuable indicator for evaluating sedimentary environments. Statistical analyses suggest that cherts deposited at continental margins typically exhibit a La_N/Ce_N ratio close to 1. On the other hand, cherts formed at spreading ridges tend to have a higher ratio, often exceeding 3.5 and in pelagic environments, the La_N/Ce_N ratio generally falls within the range of 2−3.[34] The La_N/Ce_N results suggest that the siliceous rocks fall within a continental margin. The shallow sea area, which is relatively stable, is rich in LREE, while the deep sea area and the tectonic activity region lack REEs in sediments.[61,62] The study area exhibits characteristics of LREE enrichment and HREE depletion, indicating that it mainly consists of shallow continental shelf sediment. This finding is consistent with the epeiric sea environment of the entire Yangtze platform during the late Permian.[13]

In addition to the reactive sedimentary tectonic setting, black siliceous rocks also record the redox properties of the water column. Previous studies indicate that the occurrence state and content of variable valence elements such as U, Mo, and V in sediments vary due to different redox conditions.[62] Therefore, these elements play a crucial role in evaluating the redox status of water during the deposition phase. Typically, U exists in water primarily as dissolved U^{6+} in an oxidized setting.[63] Conversely, in a reducing environment, U^{6+} is usually converted into insoluble U^{4+} and is concentrated in sediments. Hence, during reducing environmental conditions, mudstone tends to exhibit a higher U content.[64] Regarding vanadium, soluble V(V) is reduced to V(IV) under conditions such as reductive conditions, forming insoluble hydroxides ($VO(OH)^{3-}$). Under euxinic conditions, the presence of free H_2S leads to a further reduction of V(IV) to V(III). V(III) can be absorbed by geoporphyrin complexes or precipitate as solid oxides.[65−68] Mo is another redox-sensitive element that is often linked to its presence in sulfidic or euxinic environments. In these environments, H_2S in seawater or porewater can cause the transformation of dissolved molybdate into particle-reactive thiomolybdates, which ultimately accumulate in sediments.[69−71] Research on contemporary marine sediments demonstrates that sedimentary concentrations of Mo frequently exceed 100 ppm in the presence of persistent euxinic conditions. Additionally, concentrations of Mo fluctuate between 25 and 100 ppm in situations of intermittent euxinic conditions. Finally, Mo concentrations remain below 25 ppm when noneuxinic conditions prevail.[72−74]

In addition, the $EF_{Mo}-EF_U$ covariations have been applied to deduce the paleoenvironment and hydrological conditions reconstruction.[33,75,76]

The EF_U, EF_{Mo}, and EF_V ratios of 18 samples from the Putaoling section of the Dalong Formation range from 7.26 to 60.23 (with a mean of 27.39), 10.13 to 1310.25 (with a mean of 310.13), and 0.75 to 26.14 (with a mean of 5.97), respectively. These redox signals suggest an anoxic/euxinic water column during deposition. Similarly, the EF_U, EF_{Mo}, and EF_V ratios of 23 samples from the Fantiansi section of the Dalong Formation range from 9.58 to 158.45 (with a mean value of 45.76), 27.65 to 1425.63 (with a mean value of 290.62), and 1.30 to 19.99 (with a mean value of 9.94), respectively, which may reflect a euxinic environment. Furthermore, most points of the EF_{Mo}/EF_U values are situated fall within a zone around three times of the modern seawater (Figure 8), providing further indication of the existence of a euxinic environment.

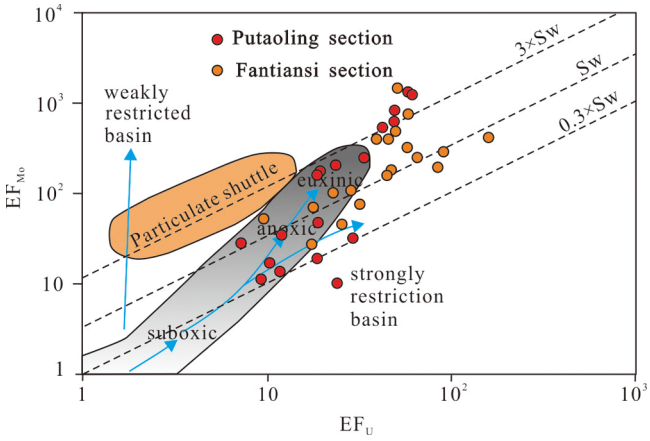

Figure 8. EF_{Mo} versus EF_U of Dalong Formation in Putaoling and Fantiansi sections. Dotted lines showing Mo/U molar ratios equal to the seawater values (0.3 × SW, 1 × SW, 3 × SW). (Base map adapted with permission from ref 76. Copyright 2009 Elsevier.)

In conclusion, our study suggests that the predominantly deposited black siliceous rocks of the Dalong Formation in the Lower Yangtze region occurred within a continental margin setting. The water column during the Late Permian period experienced a widespread anoxic/euxinic environment, which facilitated the preservation of organic matter following biological decay. This particular environment plays a crucial role in the formation of organic-rich mudstones and holds considerable research significance.

5.3. Formation Mechanism of Siliceous Rocks. During the Late Permian, South China was situated in the low latitude tropical climate zone.[3] The region had a hot climate and relatively high primary productivity,[13,14,77] creating an ideal environment for the flourishing of siliceous zooplankton. Furthermore, the Ancient Tethys Sea, due to its paleogeographic location, mainly controlled by the periodic melting of Arctic Ocean glaciers,[1,2] experienced significant upwelling at its eastern edge.[13,14,77,78] Upwelling is responsible for bringing an abundance of Mo, Ni, Cu, Zn, and P nutrients and dissolved silica in deepwaters to the surface. In the Yangtze block, stratified siliceous rocks formed by upwelling can be found, such as in the upper Permian Gufeng Formation.[79] Upwelling has also been associated with phosphorite formations in North America[1] and the Upper Permian formations in the Sverdrup Basin in the

https://doi.org/10.1021/acsomega.3c08384
ACS Omega 2024, 9, 17848−17859

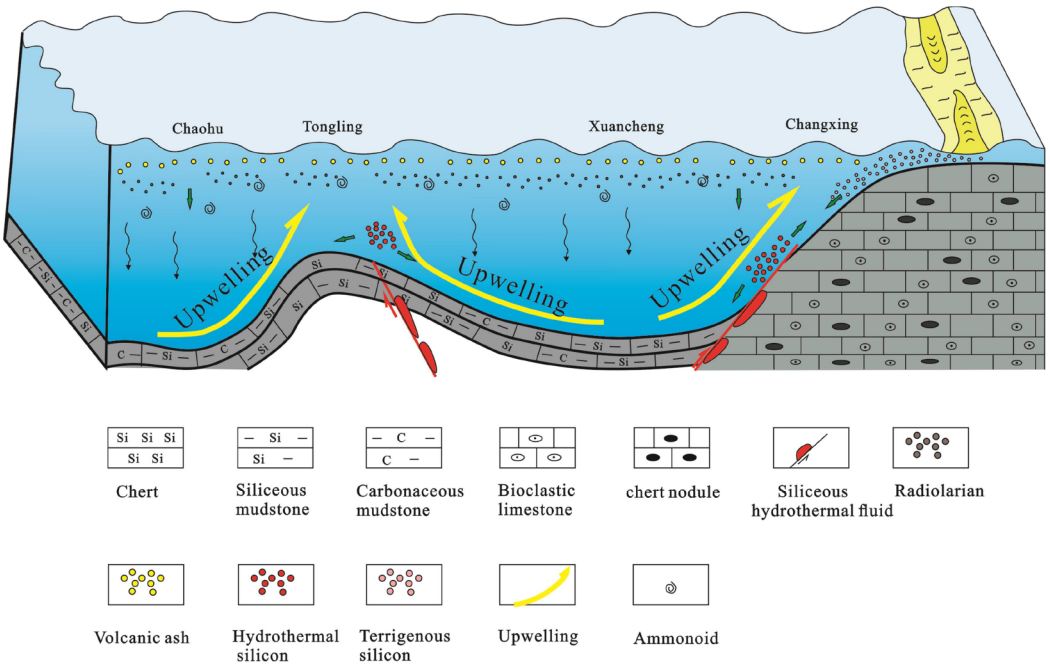

Figure 9. Model of the formation of the Dalong Formation siliceous rocks in the Lower Yangtze region.

Canadian Arctic.[80] Meanwhile, the warm-humid climate promoted the biogeochemical effect, making the chemical weathering degree of the mother rock increase, with increasing import of terrigenous silicon and nutrients into the ocean.[15]

The Permian of South China was characterized by a geotectonic background dominated by stretching effects, which promoted basement fracture and synsedimentary fracture activities. Additionally, intense volcanic activities resultd in the upwelling of magma along large fractures or synsedimentary fractures.[81] Notably, the Emeishan Large Igneous Province (ELIP) was renowned and attributed to mantle plume uplift.[82,83] Although the Lower Yangtze region was not in the basalt eruption area of Emei Mountain Basalt, Emei Tafrogeny which was closely related to it, has existed throughout the entire Yangtze region until the end of the Early Triassic.[84,85] The Fantiansi section in this study was located in the Tongling area, and it is just located at the edge of the platform. During the reactivation of the fracture, the platform edge was often accompanied by synsedimentary fracture, with deep-seated magma surging along the fracture and mixed with the infiltrated seawater, resulting in the migration of hot water to relatively shallow areas with large amounts of SiO_2 dissolved.

Regional volcanism may also play a role in the formation of cherts. Figure 2D illustrates the presence of numerous volcanic ash layers within the Putaoling section with up to 10 layers identified. It was worth noting that these layers are not only prevalent in the Jingxian, Xuancheng, Chaohu, and Tongling areas in the Lower Yangtze region[86,87] but also in the South China or Paleo-Tethys region, as evidenced by previous studies.[3,28] The submarine weathering of volcanic ash can enhance nutrient flux, including essential elements such as P, Cu, Zn, and Ni. These elements were crucial for supporting various life forms on Earth, as they played a fundamental role in numerous metabolic processes and contributed to the formation of skeletal material.[34] Abundant nutrient flux was beneficial for the proliferation of siliceous zooplankton, which led to the production of siliceous sediments through the sinking of silica-rich organisms. During the late Permian, the global atmospheric CO_2 content was notably high, ranging from 7 to 8%.[88] The increase in atmospheric CO_2 concentrations results in higher levels of $CO_{2\,(aq)}$ at the sea surface. Simultaneously, the decay of organic matter in the siliceous biota consumes a significant amount of dissolved oxygen in seawater, leading to anoxic in the water column. This process releases CO_2 into seawater, causing an increase in its CO_2 concentration. As organic matter sinks, it undergoes further decomposition within the sediment during the bacterial sulfate reduction (BSR) phase, creating euxinic conditions (Figure 8). Additionally, intense Emei Tafrogeny, with magma upwelling along major or coeval fractures, contributes to the release of CO_2 into seawater, altering its chemical properties and lowering pH.[89] Siliceous Marine organisms can grow in acidic waters and reproduce quickly in a stress-free environment. The ocean acidification event provided favorable chemical conditions for the preservation of silica.

To summarize, nutrients from coastal upwelling, volcanoes, hydrothermal liquid, and land sources jointly lead to the improvement of marine primary productivity in the Changhsingian stage, with mass multiplication of plankton such as silicon, algae, and bacteria, the ocean acidification event provided favorable chemical conditions for the preservation of silica, which eventually result in Dalong Formation siliceous rocks (Figure 9).

6. CONCLUSIONS

The petrological and geochemical characteristics of black siliceous rocks in the Dalong Formation were studied in the Chaohu Putaoling section and the Tongling Fantiansi section in the Lower Yangtze region and their implications for Permian ocean chemistry. The main conclusions are as follows:

1. The genesis of siliceous rocks of Dalong Formation in the Lower Yangtze region is relatively complex. A large number of radiolarian siliceous fossils have been observed under the microscope, with high Si_{XS} content and Al /(Al + Fe + Mn) characteristics, implying that siliceous rocks

https://doi.org/10.1021/acsomega.3c08384
ACS Omega 2024, 9, 17848−17859

are mainly of biological origin in this region. The low MgO content in the Fantiansi section of the Tongling area indicates the influence of regional hydrothermal fluids. The correlation between Al_2O_3 and TiO_2, as well as SiO_2/Al_2O_3, indicates that the deposition period of the Dalong Formation was significantly influenced by the continuous input of terrigenous materials.

2. The black bedded siliceous rocks of the Dalong Formation were predominantly deposited in a continental margin setting. The water column experienced widespread anoxic/euxinic during the Late Permian, which aided in the preservation of organic matter following biological decay.
3. In the Late Permian, South China experienced a hot tropical climate, coastal upwelling and continental weathering-enriched marine nutrients, fostering high primary productivity, benefiting abundant siliceous zooplankton. Volcanic and regional hydrothermal activityfurther enhanced nutrient flux, and the simultaneous ocean acidification event provided favorable chemical conditions for the preservation of silica, leading to the formation of siliceous rocks in the Dalong Formation.

AUTHOR INFORMATION

Corresponding Authors

Chaogang Fang − *Nanjing Center, China Geological Survey, 210016 Nanjing, China;* orcid.org/0000-0002-7195-2960; Email: fangchaogang206@163.com

Yinghai Guo − *School of Resources and Geosciences, China University of Mining and Technology, 221116 Xuzhou, China;* Email: guoyh@cumt.edu.cn

Authors

Xue Gao − *School of Resources and Geosciences, China University of Mining and Technology, 221116 Xuzhou, China; Nanjing City Vocational college, 211200 Nanjing, China*

Qi Liu − *Sichuan Liwu Copper Co., Ltd., 610091 Chengdu, China*

Complete contact information is available at: https://pubs.acs.org/10.1021/acsomega.3c08384

Notes

The authors declare no competing financial interest.

ACKNOWLEDGMENTS

This work was supported by the Fundamental and Commonweal Geological Survey of Oil and Gas of China [DD 20221662] and the National Natural Science Foundation of China [41772130].

REFERENCES

(1) Murchey, B. L.; Jones, D. L. A mid-Permian chert event: widespread deposition of biogenic siliceous sediments in coastal, island arc and oceanic basins. *Palaeogeography, Palaeoclimatology, Palaeoecology* **1992**, *96*, 161−174.

(2) Beauchamp, B.; Baud, A. Growth and demise of Permian biogenic chert along northwest Pangea: evidence for end-Permian collapse of thermohaline circulation. *Palaeogeography, Palaeoclimatology, Palaeoecology* **2002**, *184*, 37−63.

(3) Yin, H. F.; Wu, S. B.; Du, Y. S.; Peng, Y. Q. South China defined as part of Tethyan archipelagic ocean system. *Earth Sci. J. China Univ. Geosci.* **1999**, *24*, 1−12. (in Chinese with English abstract)

(4) Kametaka, M.; Takebe, M.; Nagai, H.; Zhu, S.; Takayanagi, Y. Sedimentary environments of the Middle Permian phosphorite−chert complex from the northeastern Yangtze platform, China; the Gufeng Formation: a continental shelf radiolarian chert. *Sedimentary Geology* **2005**, *174*, 197−222.

(5) Qiu, Z.; Wang, Q. C. Geochemical evidence for submarine hydrothermal origin of the Middle-Upper Permian chert in Laibin of Guangxi. *China. Science China: Earth Sciences* **2011**, *54*, 1011−1023. (in Chinese with English abstract)

(6) Tian, Y. T.; Feng, Q. L.; Li, Q. The petrogenesis and sedimentary environment of the bedded cherts from upper Permian Dalong formation, Southwest Guangxi. *Acta Sediment. Sin.* **2007**, *25*, 671−677. (in Chinese with English abstract)

(7) Feng, Q.; Algeo, T. J. Evolution of oceanic redox conditions during the Permo-Triassic transition: Evidence from deepwater radiolarian facies. *Earth-Science Reviews* **2014**, *137*, 34−51.

(8) Erwin, D. H. The Permo−Triassic extinction. *Nature* **1994**, *367*, 231−236.

(9) Isozaki, Y. Permo-Triassic boundary superanoxia and stratified superocean: records from lost deep sea. *Science* **1997**, *276*, 235−238.

(10) Isozaki, Y.; Kawahata, H.; Minoshima, K. The Capitanian (Permian) Kamura cooling event: the beginning of the Paleozoic−Mesozoic transition. *Palaeoworld* **2007**, *16*, 16−30.

(11) Shen, S. Z.; Ramezani, J.; Chen, J.; Cao, C. Q.; Erwin, D. H.; Zhang, H.; Xiang, L.; Schoepfer, S. D.; Henderson, C. M.; Zheng, Q. F. A sudden end-Permian mass extinction in South China. *GSA Bulletin* **2019**, *131*, 205−223.

(12) Chao, T. T.; Song, Z. G.; Wang, S. B.; Xia, J. Physical property characteristics and controlling factors of Permian shale reservoir in the Lower Yangtze Platform. *Nat. Gas Geosci.* **2015**, *26*, 341−351.

(13) Liao, Z. W.; Hu, W. X.; Fu, X. G.; Hu, Z. Y. Geochemistry of upper Permian siliceous rocks from the Lower Yangtze region, southeastern China: implications for the origin of chert and Permian ocean chemistry. *Petroleum Science* **2019**, *16*, 252−266.

(14) Wu, W.; Liu, W.; Mou, C.; Liu, H.; Qiao, Y.; Pan, J.; Ning, S.; Zhang, X.; Yao, J.; Liu, J. Organic-rich siliceous rocks in the upper Permian Dalong Formation (NW middle Yangtze): Provenance, paleoclimate and paleoenvironment. *Marine and Petroleum Geology* **2021**, *123*, No. 104728.

(15) Ding, J.; Zhang, J.; Huo, Z.; Shen, B.; Shi, G.; Yang, Z.; Li, X.; Li, C. Controlling factors and formation models of organic matter accumulation for the Upper Permian Dalong Formation black shale in the Lower Yangtze region, South China: Constraints from geochemical evidence. *ACS omega* **2021**, *6*, 3681−3692.

(16) Yao, X.; Zhou, Y.; Li, S.; Li, D. Research status and advances in chert and Permian chert event. *Adv. Earth Sci.* **2013**, *28*, 1189. (in Chinese with English abstract)

(17) Cheng, C.; Li, S.; Zhao, D.; Yan, L. Geochemical characteristics of the Middle-Upper Permian bedded cherts in the northern margin of the Yangtze block and its response to the evolution of paleogeography and paleo-ocean. *Bull. Mineral. Petrol. Geochem.* **2015**, *34*, 155−166. (in Chinese with English abstract)

(18) Yang, Y. C. *Research on Geochemical Characteristics and Formative Factors of Cherts in the Dalong Formation of the Shangjianggou Area, Northwestern Sichuan Basin*. Chengdu University of Technology 2015 (in Chinese with English abstract).

(19) Zhang, B.; Cao, J.; Mu, L.; Yao, S.; Hu, W.; Huang, H.; Lang, X.; Liao, Z. The Permian chert event in South China: new geochemical constraints and global implications. *Earth-Science Reviews* **2023**, *244*, No. 104513.

(20) Wang, X. P.; Mou, C. L.; Xiao, Z. H.; Zheng, B. S.; Chen, Y.; Wang, Q. Y.; Liu, W. Q. Genesis of black rock series of Upper Permian Dalong Formation in Hefeng area, Hubei province: an evidence from the analysis of element geochemistry in well HD1. *Acta Petrol. Sin.* **2018**, *39*, 1355. (in Chinese with English abstract)

(21) Xu, Y. T. Genetic geochemistry for the bedded silicalite in the late Permian Dalong formation and its sedimentary setting in southeastern Hubei. *J. Guilin Inst. Technol.* **1997**, *17*, 204−212. (in Chinese with English abstract)

(22) Yu, H.; Chen, D. Z.; Wei, H. Y.; Wang, J. G. Origin of bedded chert and organic matter accumulation in the Dalong Formation of Upper Permian in western Hubei Province. *Acta Petrol. Sin.* **2012**, *28*, 1017−1027.
(23) Shi, C.; Cao, J.; Bao, J.; Zhu, C.; Jiang, X.; Wu, M. Source characterization of highly mature pyrobitumens using trace and rare earth element geochemistry: Sinian−Paleozoic paleo-oil reservoirs in South China. *Org. Geochem.* **2015**, *83*, 77−93.
(24) Shi, C.; Cao, J.; Tan, X.; Luo, B.; Zeng, W.; Hong, H.; Huang, X.; Wang, Y. Hydrocarbon generation capability of Sinian−Lower Cambrian shale, mudstone, and carbonate rocks in the Sichuan Basin, southwestern China: Implications for contributions to the giant Sinian Dengying natural gas accumulation. *AAPG Bulletin* **2018**, *102*, 817−853.
(25) Yang, Z. Y. *Stratigraphy and Fauna of the Permian-Triassic Boundary in South China.* Geological Press, **1987** (in Chinese with English abstract).
(26) Anhui Provincial Geological Bureau. *The Regional Geology of Anhui Province*. Geological Publishing House: Beijing, 1987 (in Chinese with English abstract)
(27) Du, Y.; Li, S.; Kong, W.; Li, H. The Permian sedimentary facies and depositional environment analysis in the Jingxian−Nanling region of Anhui. *J. Stratigraphy* **2010**, *4*, 431−444. (in Chinese with English abstract)
(28) Shen, J.; Algeo, T. J.; Hu, Q.; Zhang, N.; Zhou, L.; Xia, W. C.; Xie, S.; Feng, Q. Negative C-isotope excursions at the Permian-Triassic boundary linked to volcanism. *Geology* **2012**, *40*, 963−966.
(29) Feng, Q.; Gu, S. Uppermost Changxingian (Permian) radiolarian fauna from southern Guizhou, southwestern China. *Journal of Paleontology* **2002**, *76*, 797−809.
(30) Feng, Z. Z.; He, Y. B.; Wu, S. H. Permian lithofacies paleogeography in the Middle and Lower Yangtze region. *Acta Sedimentol. Sin.* **1993**, *11*, 13−24. (in Chinese with English abstract)
(31) Taylor, S. R.; Mclennan, S. M. *The Continental Crust: its Composition and Evolution.* Blackwell: Oxford, UK, 1985; pp 1−311.
(32) Calvert, S.; Ersen, T. Geochemistry of recent oxic and anoxic marine sediments: implications for the geological record. *Mar. Geol.* **1993**, *113*, 67−88.
(33) Piper, D.; Perkins, R. A modern vs. Permian black shale—the hydrography, primary productivity, and water-column chemistry of deposition. *Chemical geology* **2004**, *206*, 177−197.
(34) Tribovillard, N.; Algeo, T. J.; Lyons, T.; Riboulleau, A. Trace metals as paleoredox and paleoproductivity proxies: an update. *Chemical geology* **2006**, *232*, 12−32.
(35) Murray, R. W. Chemical criteria to identify the depositional environment of chert: general principles and application. *Sedimentary Geology* **1994**, *90*, 213−232.
(36) Sugisaki, R.; Yamamoto, K.; Adachi, M. Triassic bedded cherts in central Japan are not pelagic. *Nature* **1982**, *298*, 644−647.
(37) Takebe, M.; Kametaka, M.; Takayanagi, Y.; Mimura, K.; Sugitani, K.; Yamamoto, K. Origin and deposition of organic matter in continental chert of the Middle Permian Gufeng Formation in the northeastern Yangtze platform. *Sedimentary Geology* **2007**, *201*, 141−148.
(38) Yu, Y.; Lin, L.; Deng, X.; Wang, Y.; Li, Y.; Guo, Y. Geochemical features of the Middle−Upper Permian cherts and implications for origin, depositional environment in the Sichuan Basin. *SW China. Geological Journal* **2020**, *55*, 1493−1506.
(39) Yan, S. T.; Tan, C. H.; Qin, M.; Li, H.; Duan, Y. H. Geochemical Characteristics and Geological Significance of Permian−Triassic Siliceous rocks in Litang Area Sichuan Province. *Acta Geosci. Sin.* **2020**, *41*, 504−514. (in Chinese with English abstract)
(40) Lin, L.; Yu, Y.; Gao, J.; Hong, W. The origin and geochemical characteristics of Permian chert in the Eastern Sichuan Basin. *China. Carbonates and Evaporites* **2018**, *33*, 613−624.
(41) Zhang, C. L.; Zhou, D. W.; Lu, G. X. Geochemical characteristics and sedimentary environments of cherts from kumishi ophiolitic melange in southern Tianshan. *Acta Petrol. Sin.* **2006**, *22*, 57−64. (in Chinese with English abstract)
(42) Roaldset, E. Rare earth elements in different size fractions of a marine quick clay from Ullensaker, and a till from Upper Numedal. *Norway. Clay Minerals* **1979**, *14*, 229−240.
(43) Koporulin, V. I.; Lyapunov, S. M.; Seredin, V. V. Rare earth elements in the clay fraction of coaliferous sediments of the Arkagalinskoe (Magadan district) and Dolinskoe (Sakhalin Island) coalfields. *Lithology and Mineral Resources* **2009**, *44*, 482−496.
(44) Wang, S.; Zou, C.; Dong, D.; Wang, Y.; Huang, J.; Guo, Z. Biogenic silica of organic-rich shale in Sichuan Basin and its significance for shale gas. *Acta Sci. Nat. Univ. Pek.* **2014**, *50*, 476−486.
(45) Holdaway, H. K.; Clayton, C. J. Preservation of shell microstructure in silicified brachiopods from the Upper Cretaceous Wilmington Sands of Devon. *Geological Magazine* **1982**, *119*, 371−382.
(46) Ross, D. J.; Bustin, R. M. Investigating the use of sedimentary geochemical proxies for paleoenvironment interpretation of thermally mature organic-rich strata: Examples from the Devonian−Mississippian shales, Western Canadian Sedimentary Basin. *Chem. Geol.* **2009**, *260*, 1−19.
(47) Rona, P. A. Criteria for recognition of hydrothermal mineral deposits in oceanic crust. *Economic Geology* **1978**, *73*, 135−160.
(48) Peng, J.; Ying, H. S.; Xia, W. J. Geochemical criteria of the Upper Sinian cherts of hydrothermal origin on the southeast continental margin of the Yangtze plate. *Acta Geochim.* **2000**, *19*, 217−226.
(49) Yamamoto, K. Geochemical characteristics and depositional environments of cherts and associated rocks in the Franciscan and Shimanto Terranes. *Sedimentary Geology* **1987**, *52*, 65−108.
(50) Boström, K. *Genesis of Ferromanganese Deposits-Diagnostic Criteria for Recent and Old Deposits, Hydrothermal Processes at Seafloor Spreading Centers*. Springer, 1983; pp 473−489.
(51) Ren, G.; Wang, P.; Zhang, L.; Zhang, B.; Dai, J. Discussion on geochemical characteristics and sedimentary environment of the Fransnian radiolarian chert in Southeastern Yunnan. *Geol. Rev.* **2011**, *57*, 505−514. (in Chinese with English abstract)
(52) He, Z. W.; Yang, R. D.; Gao, J.; Chen, W.; Liu, S.; Zhang, W. F. The geochemical characteristics and sedimentary environment of manganese-bearing rock series of Daotuo manganese deposit, Songtao County of Guizhou Province. *Geol. Rev.* **2014**, *60*, 1061−1075. (in Chinese with English abstract)
(53) Gao, J.; Yang, R.; Xu, H.; Zhang, X.; Feng, K.; Zheng, L. Genesis of Permian sedimentary manganese deposits in Zunyi, Guizhou Province, SW China: Constraints from geology and elemental geochemistry. *Journal of Geochemical Exploration* **2018**, *192*, 142−154.
(54) Chen, H.; Xie, X.; Hu, C.; Huang, J.; Li, H. Geochemical characteristics of Late Permian sediments in the Dalong Formation of the Shangsi Section, Northwest Sichuan Basin in South China: implications for organic carbon-rich siliceous rocks formation. *Journal of Geochemical Exploration* **2012**, *112*, 35−53.
(55) Adachi, M.; Yamamoto, K.; Sugisaki, R. Hydrothermal chert and associated siliceous rocks from the northern Pacific their geological significance as indication od ocean ridge activity. *Sedimentary Geology* **1986**, *47*, 125−148.
(56) Cheng, C.; Li, S.; Zhao, D.; Yan, L. Geochemical characteristics of the Middle−Upper Permian bedded cherts in the northern margin of the Yangtze Block and its response to the evolution of paleogeography and paleo-ocean. *Bull. Mineral., Petrol. Geochem.* **2015**, *34*, 155−166. (in Chinese with English abstract)
(57) Dong, Y.; Xu, S.; Wen, L.; Chen, H.; Fu, S.; Zhong, Y.; Wang, J.; Zhu, P.; Cui, Y. Tectonic control of Guadalupian-Lopingian cherts in northwestern Sichuan basin, South China. *Palaeogeography, Palaeoclimatology, Palaeoecology* **2020**, *557*, No. 109915.
(58) Murray, R. W.; Buchholtz, T.; Brink, M. R.; David, L. J.; David, C. G.; Price, G.; Russ, I. I. I. Rare earth elements as indicators of different marine depositional environments in chert and shale. *Geology* **1990**, *3*, 268.
(59) Murray, R. W.; Ten brink, M. R. B.; Gerlach, D. C.; Russ, G. P., III; Jones, D. L. Rare earth, major, and trace elements in chert from the Franciscan Complex and Monterey Group, California: Assessing REE sources to fine-grained marine sediments. *Geochim. Cosmochim. Acta* **1991**, *55*, 1875−1895.

https://doi.org/10.1021/acsomega.3c08384
ACS Omega 2024, 9, 17848−17859

(60) Gromet, L. P.; Haskin, L. A.; Korotev, R. L.; Dymek, R. F. The "North American shale composite": Its compilation, major and trace element characteristics. *Geochimica et cosmochimica acta* **1984**, *48*, 2469−2482.
(61) Hu, J.; Li, Q.; Li, J.; Huang, J.; Ge, D. Geochemical characteristics and depositional environment of the Middle Permian mudstones from central Qiangtang Basin, northern Tibet. *Geological Journal* **2016**, *51*, 560−571.
(62) Crusius, J.; Calvert, S.; Pedersen, T.; Sage, D. Rhenium and molybdenum enrichments in sediments as indicators of oxic, suboxic and sulfidic conditions of deposition. *Earth and Planetary Science Letters* **1996**, *145*, 65−78.
(63) Skomurski, F. N.; Ilton, E. S.; Engelhard, M. H.; Arey, B. W.; Rosso, K. M. Heterogeneous reduction of U^{6+} by structural Fe^{2+} from theory and experiment. *Geochim. Cosmochim. Acta* **2011**, *75*, 7277−7290.
(64) Anderson, O.; Greene, F. The characterization and comparative analysis of high-molecular-weight glutenin genes from genomes A and B of a hexaploid bread wheat. *Theor. Appl. Genet.* **1989**, *77*, 689−700.
(65) Wilford, J. A weathering intensity index for the Australian continent using airborne gamma-ray spectrometry and digital terrain analysis. *Geoderma* **2012**, *183*, 124−142.
(66) Breit, G. N.; Wanty, R. B. Vanadium accumulation in carbonaceous rocks: a review of geochemical controls during deposition and diagenesis. *Chem. Geol.* **1991**, *91*, 83−97.
(67) Wanty, R. B.; Goldhaber, M. B. Thermodynamics and kinetics of reactions involving vanadium in natural systems_ Accumulation of vanadium in sedimentary rocks. *Geochim. Cosmochim. Acta* **1992**, *56*, 1471−1483.
(68) Ge, X.; Chen, D.; Zhang, G.; Huang, T.; Liu, M.; El-shafeiy, M. Marine redox evolution and organic accumulation in an intrashelf basin, NE Sichuan Basin during the Late Permian. *Marine and Petroleum Geology* **2022**, *140*, No. 105633.
(69) Helz, G. R.; Miller, C. V.; Charnock, J. M.; Mosselmans, J. F. W.; Pattrick, R. A. D.; Garner, C. D.; Vaughan, D. J. Mechanism of molybdenum removal from the sea and its concentration in black shales: EXAFS evidence. *Geochim. Cosmochim. Acta* **1996**, *60*, 3631−3642.
(70) Tribovillard, N.; Algeo, T. J.; Baudin, F.; Riboulleau, A. Analysis of marine environmental conditions based on molybdenum−uranium covariation - applications to Mesozoic paleoceanography. *Chem. Geol.* **2012**, *324*−*325*, 46−58.
(71) Liu, W.; Liu, M.; Yang, T.; Liu, X.; Them, T. R.; Wang, K.; Bian, C.; Meng, Q.; Li, Y.; Zeng, X.; Zhao, W. Organic matter accumulations in the Santonian-Campanian (Upper Cretaceous) lacustrine Nenjiang shale (K_2n) in the Songliao Basin, NE China: Terrestrial responses to OAE3? *International Journal of Coal Geology* **2022**, *260*, No. 104069.
(72) Scott, C.; Lyons, T. W. Contrasting molybdenum cycling and isotopic properties in euxinic versus non-euxinic sediments and sedimentary rocks: refining the paleoproxies. *Chem. Geol.* **2012**, *324*−*325*, 19−27.
(73) Liu, M.; Chen, D.; Zhou, X.; Yuan, W.; Jiang, M.; Liu, L. Climatic and oceanic changes during the Middle-Late Ordovician transition in the Tarim Basin, NW China and implications for the Great Ordovician Biodiversification Event. *Palaeogeography, Palaeoclimatology, Palaeoecology* **2019**, *514*, 522−535.
(74) Liu, M.; Chen, D.; Jiang, L.; Stockey, R. G.; Aseal, D.; Zhang, B.; Liu, K.; Yang, X.; Yan, D.; Planavsky, N. J. Oceanic anoxia and extinction in the latest Ordovician. *Earth and Planetary Science Letters* **2022**, *588*, No. 117553.
(75) Algeo, T. J.; Lyons, T. W. Mo-total organic carbon covariation in modern anoxic marine environments: implications for analysis of paleoredox and paleohydrographic conditions. *Paleoceanography* **2006**, *21*, 1−23.
(76) Algeo, T. J.; Tribovillard, N. Environmental analysis of paleoceanographic systems based on molybdenum−uranium covariation. *Chem. Geol.* **2009**, *268*, 211−225.
(77) Wu, Z.; He, S.; Li, X.; Liu, X.; Zhai, G.; Huang, Z.; Yang, W. Comparative study on pore structure characteristics of marine and transitional facies shales: A case study of the Upper Permian Longtan Formation and Dalong Formation in the Lower Yangtze area, south China. *J. Pet. Sci. Eng.* **2022**, *215*, No. 110578.
(78) Kidder, D. L.; Worsley, T. R. Causes and consequences of extreme Permo-Triassic warming to globally equable climate and relation to the Permo-Triassic extinction and recovery. *Palaeogeography, Palaeoclimatology, Palaeoecology* **2004**, *203*, 207−237.
(79) Wei, H.; Yu, H.; Wang, J.; Qiu, Z.; Xiang, L.; Shi, G. Carbon isotopic shift and its cause at the Wuchiapingian−Changhsingian boundary in the Upper Permian at the Zhaojiaba section, South China: evidences from multiple geochemical proxies. *Journal of Asian Earth Sciences* **2015**, *105*, 270−285.
(80) Beauchamp, B.; Grasby, S. E. Permian lysocline shoaling and ocean acidification along NW Pangea led to carbonate eradication and chert expansion. *Palaeogeography, Palaeoclimatology, Palaeoecology* **2012**, *350*, 73−90.
(81) Liang, D. Y.; Nie, Z. T.; Song, Z. M. Extensional Dongwu movement in western margin of Yangtze region. *Earth Sci. J. China Univ. Geosci.* **1994**, *19*, 443−453. (in Chinese with English abstract)
(82) Martindale, R. C.; Foster, W. J.; Velledits, F. The survival, recovery, and diversification of metazoan reef ecosystems following the end-Permian mass extinction event. *Palaeogeography, Palaeoclimatology, Palaeoecology* **2019**, *513*, 100−115.
(83) Hong, H.; Zhao, L.; Fang, Q.; Algeo, T. J.; Wang, C.; Yu, J.; Gong, N.; Yin, K.; Ji, K. Volcanic sources and diagenetic alteration of Permian−Triassic boundary K-bentonites in Guizhou Province, South China. *Palaeogeography, Palaeoclimatology, Palaeoecology* **2019**, *519*, 141−153.
(84) Luo, Z.; Jin, Y.; Zhu, K.; Zhao, X. On Emei taphrogenesis of the upper Yangtze platform. *Geol. Rev.* **1988**, *34*, 11−23. (in Chinese with English abstract)
(85) Luo, Z. Emei Taphrogenesis and Natural Gas Prospecting Practices in Sichuan Basin. *Xing Jiang Petrol. Geol.* **2009**, *30*, 419−424. (in Chinese with English abstract)
(86) Xu, J. L.; Zhang, J. Z.; Shen, S. H.; Wang, Y. F. The discovery of altered volcanic clayrock in Late Permian strata between Longtan Formation and Dalong Formation of Jingxian area, Anhui Province. *Geol. China* **2019**, *46*, 937−938.
(87) Fang, C.; Zhang, C.; Meng, G.; Xu, J.; Xu, N.; Li, H.; Liu, M.; Liu, B. Constraints on the Accumulation of Organic Matter in the Upper Permian Dalong Formation from the Lower Yangtze Region, South China. *Acta Geologica Sinica-English Edition* **2024**, *98*, 150−167.
(88) Berner, R. A. Examination of hypotheses for the Permo-Triassic boundary extinction by carbon cycle modeling. *Proc. Natl. Acad. Sci. U. S. A.* **2002**, *99*, 4172−4177.
(89) Clapham, M. E.; Payne, J. L. Acidification, anoxia, and extinction: a multiple logistic regression analysis of extinction selectivity during the Middle and Late Permian. *Geology* **2011**, *39*, 1059−1062.

https://doi.org/10.1021/acsomega.3c08384
ACS Omega 2024, 9, 17848−17859